ELSEVIER

Tectonophysics 273 (1997) 155–167

TECTONOPHYSICS

Deep seismic structure and thermo-mechanical modelling of continental collision zones

J.P. Midgley *, D.J. Blundell

Royal Holloway, University of London, Egham, Surrey TW20 0EX, UK

Received 1 November 1995; accepted 3 April 1996

Abstract

A series of 2D thermo-mechanical models are presented which quantify crustal thickening and the resulting temperature perturbations associated with thrusting in an attempt to constrain the existence of temperatures responsible for the generation of anatectic granites in a compressional environment. Deformation is assumed to occur in the crust by a simple thrusting mechanism, the Moho acting as a detachment surface, as has been observed on deep seismic reflection data, while the more ductile sub-crustal lithosphere is assumed to behave elastically and deform in a pure shear manner. Investigated are the relative effects of the rate of crustal shortening, the distribution of radioactive elements within the crust, the reduced heat flow from the mantle, isostasy and erosion. Our results show that previous oversimplified 1D models significantly overestimate the elevated temperatures in lower crustal regions caused by radiogenic heating, and that this mechanism will only have a significant effect in regions of relatively thin lithosphere, or where there are unusually high rates of radiogenic heating in the crust. Generation of synthetic *P–T–t* data for locations deep down in the lower crust enables us to quantify the temperatures produced following a period of compressional deformation, providing insight into the time scales involved for the generation of crustal melt granites within an orogenic belt.

Keywords: thermo-mechanical; modelling; deep seismic structure; continent collision

1. Introduction

Deep seismic reflection profiles across orogenic belts related to continental collision have provided great insight into mountain-building processes. Crustal-scale thrusts have been imaged that indicate the mechanisms of crustal shortening and thickening. Orogenic belts also have a distinct form of metamorphism and often include large volumes of crust that was partially melted during orogenesis. Previous authors (e.g., England and Thompson, 1986) have shown, using simple 1D temperature–depth models, that temperatures in lower crustal regions can rise significantly as a result of increasing the amount of radiogenic heating within the crust, following crustal thickening. These models assumed a uniform value for the rate of radiogenic heating in the crust, neglected any lateral temperature perturbations, and assumed that crustal thickening occurred instantaneously. Shi and Wang (1987) and Ruppel and Hodges (1994), however, illustrated the effects of the temperature perturbations by allowing a finite time for the deformation period and by taking into account horizontal temperature gradients. Their models were based on crustal shortening only and neglected the upper mantle part of the lithosphere.

* Corresponding author.

PII S0040-1951(96)00292-2

It is also generally accepted that radiogenic heat production is not constant in the crust but decreases with depth. Hence a more thorough examination of the conditions under which large-scale crustal melting (anatexis) can occur following a period of compressional deformation of the whole lithosphere is required that takes into account the mechanisms of crustal and lithosphere shortening and thickening.

This paper presents a series of 2D thermo-mechanical models that quantify the evolution in time of the temperature perturbations that result from lithosphere shortening and thickening. The relative effects of radiogenic heating in the crust, heat from below in the sub-crustal lithosphere, isostasy and erosion are all investigated, to provide insight into the conditions under which extensive crustal melting might occur. The effects of frictional heating, previously considered by Graham and England (1976) and Johnston and White (1983), have been ignored here as this mechanism is very localised to the fault plane and hence unable to initiate extensive crustal melting in mid and lower crustal regions.

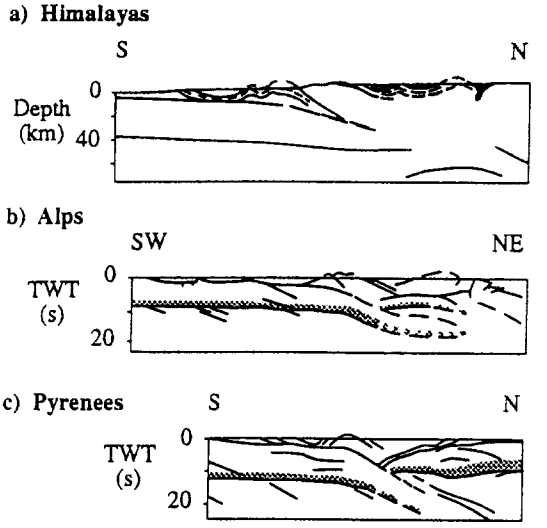

Fig. 1. Cross-sections of young collisional belts, incorporating deep seismic reflection, refraction and gravity data (from Nelson, 1992): (a) Himalayas, (b) Alps, (c) Pyrenees. Solid line Moho, observed on deep seismic reflection profiles. Dashed Moho, interpreted from wide-angle reflection–refraction–gravity data. Grey in Alps and Pyrenees sections denotes reflective lower crust.

2. Modes of crustal shortening and thickening during continental collision

Following continental collision, crustal shortening and thickening can be accommodated by various means. Evidence from deep seismic profiles across various orogenic belts indicates the range of structural styles and illustrates the mechanisms involved, as shown schematically in Fig. 1.

2.1. Young orogenic belts

The Himalayas formed as a result of a collision between India and Asia about 45 Ma (Dewey et al., 1989), creating regions of thickened crust within the Himalayan–Tibetan orogen. Following the onset of collision, India continued moving northwards at a rate of about 50 mm a^{-1} (Treloar et al., 1992) and in consequence this orogenic belt must have accommodated over 2000 km of shortening (Fig. 1a) through a combination of subduction (Butler and Coward, 1989), thickening by thrusting (Coward and Butler, 1985), homogeneous thickening (Dewey et al., 1988), and some form of lateral eastward extrusion of Tibet (England and Molnar, 1990). Collision appears to have occurred earlier in the northwest of the Himalayas than in the east where there is no evidence of the late metamorphism and leucogranite magmatism that is widely developed within the Indian and Nepalese Himalayas (Treloar et al., 1992).

Recent deep seismic reflection profiles across the Alps (Fig. 1b) have imaged the Penninic front (Bayer et al., 1987) as a band of strong reflections that cut discordantly the complex structures of the Penninic nappes, indicating a younger shear zone (Laubscher, 1992). This shear zone defines the base of an 'orogenic lid' (Laubscher, 1983) of brittle crust occupying the upper 10–20 km of a collision zone. At its base it produces a series of nappes through predominantly simple shear and, at its leading edge, frontal fold and thrust belts (Laubscher, 1992).

Thrust structures and related syn-orogenic materials of the Pyrenees, formed from the Tertiary collision between Iberian and European continents, are very well preserved and hence have been the focus of much detailed research of recent times (e.g., Muñoz, 1992). A deep seismic reflection profile across the central Pyrenees (ECORS-PYRENEES), interpreted along with surface geology and commercial seis-

mic and oil-well data, permits the construction of a reasonably well constrained lithosphere cross-section (Muñoz, 1992). The continental lower crust and lithospheric mantle appear to have been subducted, as shown in Fig. 1c.

Thrusts in the Himalayas have been observed to affect the whole of the crust, detaching from the Moho (Mattauer, 1986), whilst in the Alps, slices of lower crust are thrust into the upper mantle (Bayer et al., 1987). In the Pyrenees, however, the Iberian lower crust has remained attached to the lithospheric mantle which appears to have been subducted intact below the European lithosphere (Muñoz, 1992).

2.2. Precambrian orogenic belts

Supracrustal rocks define three major provinces of continental accretion in the southwestern United States with ages of 1.72–1.80, 1.65–1.72 and 1.1–1.2 Ga (Condie, 1982). Granitic plutons intrude all three provinces. Geochemical and Sr-isotope data provide evidence in each case of a short-lived (<100 Ma) lower-crustal source for granitic magmas. Fig. 2 shows a schematic model for the earliest collisional event (adapted from Condie, 1982). The closing of a marginal basin and collision of an offshore arc system with the Wyoming Archaean Province (Fig. 2a) was followed by the opening of a small back-arc basin underlain by continental crust (Fig. 2b). This basin then closed with the accretion of microcontinental fragments, supracrustal successions were deformed, and partial melting of the thickened crust produced granitic magmas that were syntectonically intruded (Fig. 2c). The same cycle is believed to have been repeated between 1.65 and 1.72 Ga and again between 1.1 and 1.2 Ga.

The Proterozoic Sveco-Fennian orogenic belt developed by the growth and collision of 2.0–1.8 Ga juvenile island arcs, and substantial crustal melting during the period 1.8–1.55 Ga (Windley, 1992). Post-collisional deformation in the form of thrusting and folding led to the formation of abundant crustal melt granites. The 1600-km-long, 150-km-wide Trans-Scandinavian batholith lies on the southwestern margin of the orogenic belt and may have developed over an east-dipping subduction zone (Andersson, 1991). A large-scale seismic profile FENNOLORA (Ansorge et al., 1992) that crosses it shows that

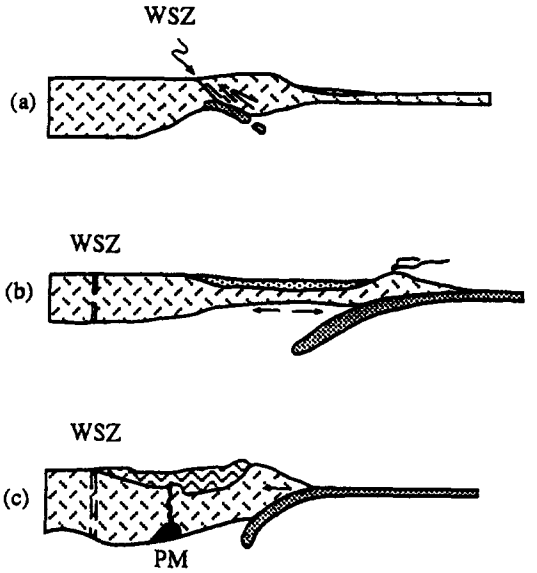

Fig. 2. Early Proterozoic continental accretionary stages for the southwestern United States (after Condie, 1982). (a) Collision of offshore arc system. (b) Opening of back-arc basin. (c) Collision and accretion leading to the formation of partial melting in the thickened crust. *WSZ* = Wyoming shear zone. *PM* = region of partial melting.

the crust thickens from 40 km to 52 km below the batholith, and this is also supported by an offshore deep seismic reflection profile, BABEL B (BABEL Working Group, 1993), which flanks the batholith. A line drawing of the unmigrated section of profile BABEL B is shown in Fig. 3. Throughout the entire section there is a general trend for reflectors to rise up from the Moho (interpreted as the base of the lower-crustal reflectivity) through the middle part of the crust, culminating in quite distinct antiformal structures at a depth of about 4 s TWT. These are interpreted as an imbricated thrust stack of crustal scale that formed as a result of a lateral compression. This created a region of thickened crust which is still preserved, the depth of the Moho increasing from just under 10 s TWT (ca. 32 km) at the southern end of the profile to about 14 s TWT (ca. 45 km) at the northern end. Above the thrust stack is a 10-km-thick zone at the top of the crust which is virtually devoid of any major reflections, representing a homogeneous region. Since granite has been found elsewhere to be transparent on seismic sections (BIRPS and ECORS, 1988), this zone could

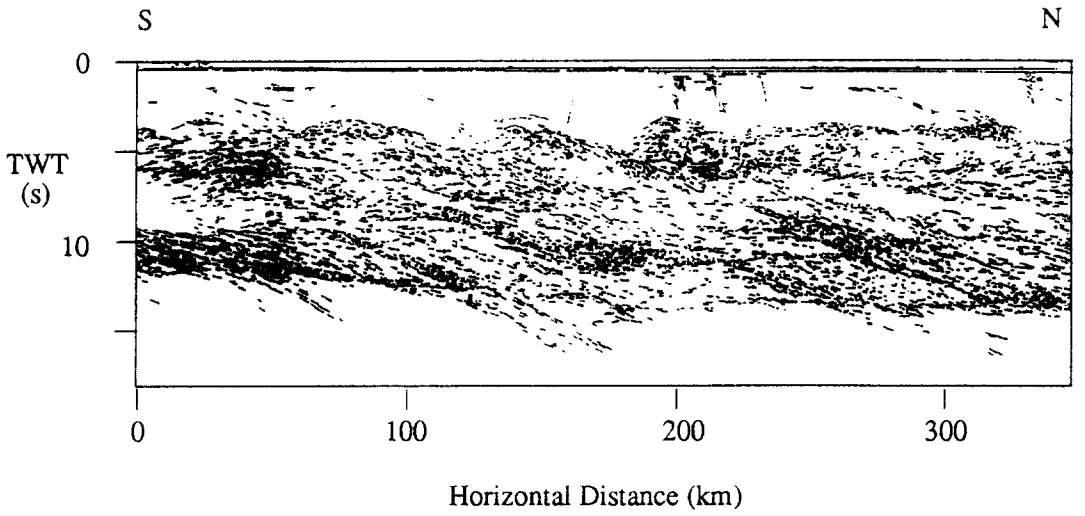

Fig. 3. Line drawing of the unmigrated deep seismic reflection profile BABEL B, imaging a series of crustal-scale thrust slices that appear to detach at the Moho.

represent the eastern flank of the Trans-Scandinavian batholith. Gravity evidence (Zuber and Öhlander, 1990) suggests that the main part of the batholith fills the bulk of the crust but it spreads laterally eastwards in the upper crust, perhaps as far as BABEL B.

The section of profile BABEL B has many similarities with that across the Canadian Cordillera (Cook et al., 1992) where crustal-scale thrusts come to surface. A crustal-scale thrust stack is also observed across the Late Proterozoic Grenville front in eastern Canada (Green et al., 1989). In both cases, there is clear evidence of lateral compression being accommodated by crustal-scale imbrication.

Although each of the examples discussed has its own specific characteristics, their common feature is the presence of thrusting on a near-crustal scale, depending on the thickness of the 'orogenic lid'. Thus it is reasonable to examine the thermal evolution of an orogenic belt by means of a thermo-mechanical model in which lateral compression results in crustal thickening through crustal-scale thrusting.

3. Mathematical model

The temperature distribution in continental crust and lithosphere is governed by the conductive loss of heat to the surface from the sub-continental mantle and from heat generated internally by radioactive decay. The variation of temperature T with time t is given by the heat conduction equation:

$$\frac{\partial T}{\partial t} = \frac{k}{\rho c_p}\nabla^2 T - \underline{u}\nabla T + \frac{A(z)}{\rho c_p} \tag{1}$$

in which k is the thermal conductivity, ρ is density, c_p is specific heat, and $A(z)$ is the rate of internal radioactive heat generation, variable with depth z. The term $k/\rho c_p$ is often referred to as the thermal diffusivity, κ.

The first term on the right-hand side of Eq. 1 represents heat transferred by conduction, the second by thermal advection due to movement of material with velocity $\underline{u}$, and the third represents the amount of heat generated in the crust by radioactivity.

In two dimensions Eq. 1 reduces to:

$$\frac{\partial T}{\partial t} = \frac{k}{\rho c_p}\left(\frac{\partial^2 T}{\partial x^2} + \frac{\partial^2 T}{\partial z^2}\right) - u_x\frac{\partial T}{\partial x} - u_z\frac{\partial T}{\partial z} + \frac{A(z)}{\rho c_p} \tag{2}$$

where x and z are the respective horizontal and depth co-ordinates and u_x and u_z are the respective horizontal and vertical velocity components.

Continental rocks have considerably more radioactive elements at surface than at depth and for various reasons (see Carslaw and Jaeger, 1959, for discussion), it is appropriate to attribute this decrease as an exponentialfunction:

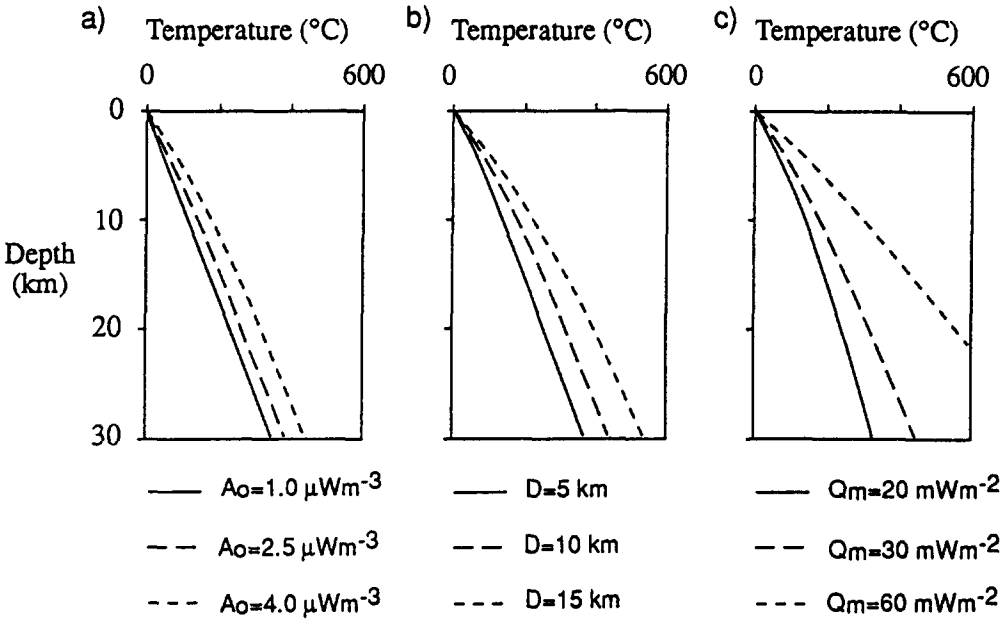

Fig. 4. Effects of thermal parameters on the equilibrium geotherm. (a) Rate of radiogenic heating in the crust, A_0 ($D = 10$ km, $Q_m = 30$ mW m^{-2}). (b) Heat generation depth scale, D ($A_0 = 2.5$ μW m^{-3}, $Q_m = 30$ mW m^{-2}). (c) Reduced heat flow, Q_m ($A_0 = 2.5$ μW m^{-3}, $D = 10$ km).

$$A(z) = A_0 e^{-\frac{z}{D}} \quad (3)$$

where A_0 is the surface radioactive heat production rate per unit mass and D is a length scale for the decrease in radioactive heat production with depth. It is assumed that radiogenic heating is confined to the crust and is negligible in the mantle.

In equilibrium, heat flow at surface Q_s is given by:

$$Q_s = Q_m + A_0 D - A_0 D e^{\frac{d}{D}} \quad (4)$$

where d is depth to the base of the crust and Q_m is the heat flow at the Moho, also known as the reduced heat flow. Similarly, the equilibrium geotherm is calculated from the temperature at depth z given by:

$$T = \frac{A_0 D^2}{k}\left(1 - e^{-\frac{z}{D}}\right) - \frac{A_0 D z}{k} e^{-\frac{d}{D}} + \frac{Q_m z}{k} \quad (5)$$

Fig. 4 shows the effects of varying the parameters Q_m, A_0 and D. The most sensitive of these is the reduced heat flow at the Moho Q_m. Table 1 shows some examples of continental heat flow from a range of crustal provinces. The values for Q_s, Q_m and D are taken from Sclater et al. (1981), while the values of A_0 have been calculated using Eq. 4. Clearly,there

Table 1
Typical continental heat flow provinces

Province	Mean Q_s (mW m^{-2})	A_0 (μW m^{-3})	D (km)	Mean Q_m (mW m^{-2})
Basin and Range (USA)	92	3.5	9.4	59
Sierra Nevada (USA)	39	2.2	10.1	17
Eastern United States	57	3.2	7.5	33
Superior Province (Canadian Shield)	39	1.3	14.4	21
United Kingdom	59	2.2	16.0	24
Western Australia	39	2.9	4.5	26
Ukrainian Shield (USSR)	37	1.7	7.1	25
Overall averages	52	2.4	10	29

is considerable variation of the parameters, including a threefold variation in Q_m.

4. Conditions required for crustal melting

Fig. 5 shows an average present-day geotherm, assuming a crustal thickness of 30 km as well as the melting curves of crustal rocks in the presence of excess water (H), from Wyllie (1992), the dehydration–melting curve of a muscovite granite (M), from Huang and Wyllie (1981), and the dehydration–melting curve of biotite (B) in metapelite from Le Breton and Thompson (1988). This clearly shows that lower-crustal temperatures are ~200°C less than the minimum required for crustal melting in water-saturated rocks, and even less than those required for fluid-absent melting. Hence, in order for crustal melting to occur, the geotherm must be perturbed sufficiently in order to cross either of the melting curves in Fig. 5.

5. Method of modelling

The model consists of a cross-section of the lithosphere with properties given in Table 2. Initially, the crust has a constant thickness of 30 km and the lithosphere has a thickness of 110 km with a temperature at its base of 1333°C, as illustrated in Fig. 6a. Lateral compression is accommodated in the crust by simple shear along a single crustal-scale thrust, and in the mantle lithosphere by pure shear, as illustrated in Fig. 6b, the surfaces of these mechanical boundaries being calculated by a finite element technique, and the distribution of radioactive elements being redefined after each time step of the model. When Airy isostatic equilibrium is maintained, the cross-section is as shown in Fig. 6c. As can be seen in Fig. 6, lateral compression results in an overall thickening of the lithosphere so that the isotherms become more widely spaced. However, the upper crust in the footwall of the thrust is buried to mid-crustal level where, although initially cool, it becomes a source of enhanced heating at this depth. The distribution of both the temperature and the radioactive heat producing elements has thus been modified by the deformation and the system is no longer in thermal equilibrium. The model then follows the time evolution of this situation. To do this, the 2D heat conduction equation (Eq. 2) has to be solved using a standard finite difference technique assuming a constant temperature at the surface and the base of the lithosphere (0°C and 1333°C, respectively) and $dT/dt = 0$ at the edges of the model. At every grid node each of the parameters listed in Table 2 is specified together with the horizontal and vertical velocities of each element of the cross-section resulting from the lithospheric shortening. In the crust, deformation in the hangingwall of

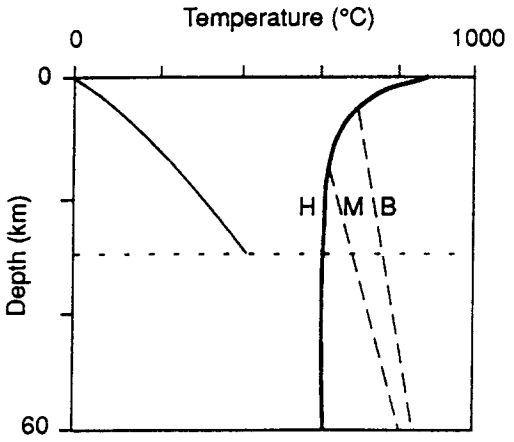

Fig. 5. Typical present-day geotherm assuming the average values in Table 2 and temperature–depth curves indicating the conditions required for partial melting of the crust. H = melting curve for crustal rocks in the presence of excess water (Wyllie, 1992); M = dehydration–melting curve of a muscovite granite (Huang and Wyllie, 1981); B = dehydration–melting curve of biotite in metapelite (Le Breton and Thompson, 1988).

Table 2
Typical parameters used in thermo-mechanical modelling

Parameter	Symbol	Value
Initial crustal thickness	d	30 km
Rate of contraction	u_x	50 mm a^{-1}
Thermal conductivity	k	2.5 W m^{-1} K^{-1}
Thermal diffusivity	κ	30 m^2 a^{-1}
Rate of radiogenic heating at surface	A_0	2.4 μW m^{-3}
Heat production depth scale	D	10 km
Density of crust	ρ_c	2800 kg m^{-3}
Density of sub-crustal lithosphere	ρ_{scl}	3300 kg m^{-3}
Density of asthenosphere	ρ_a	3200 kg m^{-3}
Reduced heat flow	Q_m	29 mW m^{-2}
Surface heat flow	Q_s	52 mW m^{-2}
Erosion rate	–	0.3 mm a^{-1}
Isostatic time constant	–	10,000 a^{-1}

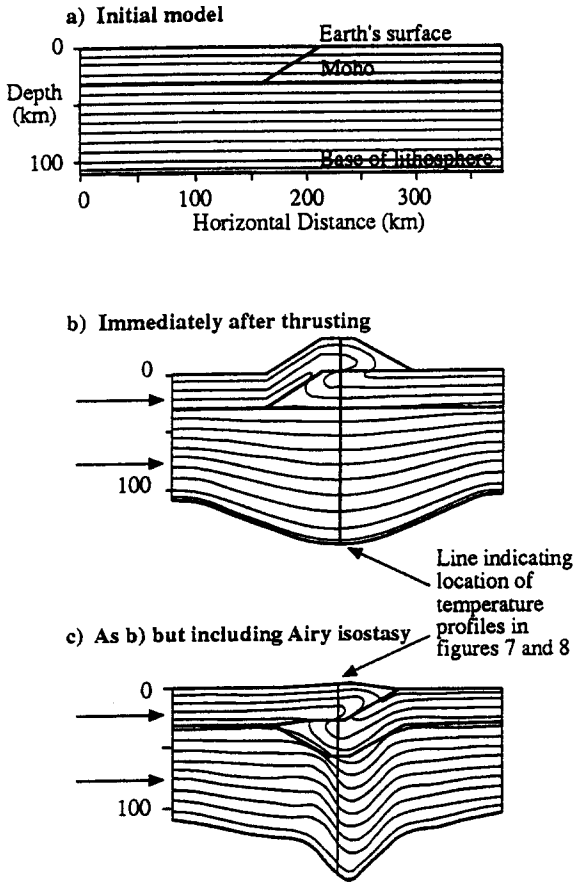

Fig. 6. Development of a thrust sheet during a period of compressional deformation and the resulting temperature perturbations (contour intervals at 100°C); the base of the lithosphere is defined by the 1333°C isotherm. (a) Initial cross-section. (b) After lateral contraction at a constant rate of 50 mm a^{-1} lasting 1.6 Ma. This results in 80 km of crustal shortening and, in the centre of the thrust sheet, the crustal thickness has been increased by a factor of two as lower crust has been emplaced on top of upper crustal material that was originally at the surface. (c) As (b) but including Airy isostatic equilibrium with a time constant of 10,000 years. The surface topography is reduced to more realistic levels but a region of thickened crust remains beneath the thrust sheet.

the thrust is assumed to be by vertical shear. Within the upper mantle lithosphere, as it shortens by pure shear in the horizontal direction, each element must thicken by the same amount in the vertical, resulting in a horizontal velocity function that decreases with horizontal distance from a fixed point, and a vertical velocity function which increases with depth from the fixed point (Waltham and Hardy, 1995). The constant of proportionality is identical for both vertical and horizontal velocities in order to conserve mass. Hence, given an initial horizontal velocity, the resulting pure shear velocity field can be easily calculated. In this model a horizontal velocity function based on a normalised, half-cosine function is preferred which produces maximum lithospheric thickening in the centre of the model, decreasing sinusoidally to the edges of the region of pure shear. The thickening of crust and lithosphere has a pronounced isostatic effect which can be determined simply by assuming Airy isostatic equilibrium, and calculating the resulting isostatic velocity using the formula derived by Waltham and Hardy (1995).

6. Analysis of model parameters

To explore their effects on thermal evolution, the controlling parameters of the model listed in Table 2 are systematically modified. In this analysis, the evolution in time of the geotherm (i.e., temperature variation with depth) in the centre of the model is followed.

6.1. Rate of shortening

If the lateral shortening is assumed to be instantaneous, the temperature of the rock in the hangingwall of the thrust is at its original surface temperature and a saw-tooth temperature distribution follows, as shown by the thick solid line in Fig. 7a. However, the sharp edges of the 'saw-tooth' are soon removed by thermal conduction and this inverted geothermal gradient has virtually disappeared 1 Ma later. Now let us consider the case whereby crustal shortening occurs over a finite time period. The dashed lines in Fig. 7 represent a rate of compression of 100 mm a^{-1}, the lithosphere shortening from 380 km to 300 km over a time span of 0.8 Ma, while the thin solid line represents a slower rate of 50 mm a^{-1}, but producing the same amount of shortening, i.e., the collisional event is assumed to last for 1.6 Ma. Fig. 7a shows that a temperature inversion still occurs, but not as sharp; the slower the rate of compression, the longer the system has to re-equilibrate. As can be seen in Fig. 7b,c, however, these differences are short-lived and by 10 Ma following the period of thrusting, all three temperature profiles are virtually identical.

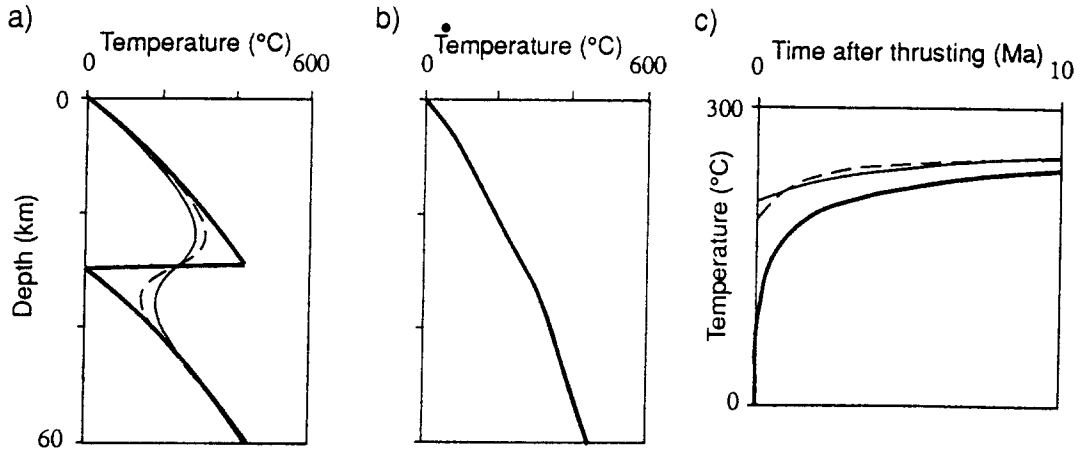

Fig. 7. Effects of the rate of shortening on the continental geotherm through the centre of the model. (a) Temperature–depth curves immediately after thrusting has occurred. The thick, solid line assumes that thickening has occurred instantaneously, resulting in a 'saw-tooth' geotherm as hot, lower-crustal material is emplaced on top of cool, surface material. The thin solid line assumes that thickening has occurred over a period of 1.6 Ma at a rate of 50 mm a^{-1}, while the intermediate dashed line represents a more rapid thickening phase of 0.8 Ma at a rate of 100 mm a^{-1} — both result in 80 km of shortening. (b) The three geotherms after 10 Ma of thermal relaxation following the end of the compression event. (c) Temperature–time paths of the three examples in (a) and (b) of a point originally at the Earth's surface.

6.2. Radioactive heating

Fig. 8a follows the evolution of the central geotherm in the model shown in Fig. 6b following lateral shortening of the lithosphere by ~20% over a time period of 1.6 Ma. The thermal parameters are listed in Table 2 and radiogenic heat production decreases exponentially within the crust. These are the values to be expected in normal continental lithosphere at the present day. In this case we observe that crustal temperatures fall short of the minimum 600°C required for partial melting of common crustal rocks under water-saturated conditions. The dashed line in Fig. 8a represents a 1D version of this model (calculated by neglecting the $\partial^2 T/\partial x^2$ term in Eq. 2). This illustrates some of the inadequacies of previous 1D models which in this example overestimates the Moho temperature by approximately 100°C. Whilst there are good reasons to assume that the rate of radiogenic heating decreases exponentially with depth in the crust, to generate thermal models, some authors (e.g., England and Thompson, 1986) have held it constant. Fig. 8b illustrates the effect of changing the distribution of radiogenic heat production within the crust from an exponential reduction with depth to a constant value, whilst keeping the total quantity of heat generated in the crust the same (i.e., the surface heat flow and the reduced heat flow are identical to those in Fig. 8a). A uniform rate of radiogenic heating throughout the crust raises the temperatures by approximately 50°C more than the same quantity of heat distributed with an exponential decrease with depth. This is as a direct consequence of the initial equilibrium geotherm assuming a uniform distribution of radiogenic heating generating higher lower-crustal temperatures than the exponentially distributed case, despite producing the same total quantity of heat within the entire crust. However, even with this increased heating, lower-crustal temperatures are still too low to induce partial melting.

6.3. Upper mantle lithosphere

The effect of lithosphere thickening in the upper mantle is that the isotherms are pushed deeper and that the temperature gradient, and hence the reduced heat flow Q_m at the Moho, is reduced from its initial value by an amount proportional to that of the shortening. Fig. 8c shows what happens if the contribution of the upper mantle lithosphere is removed. This is equivalent to keeping the reduced heat flow Q_m entering the base of the crust from the upper

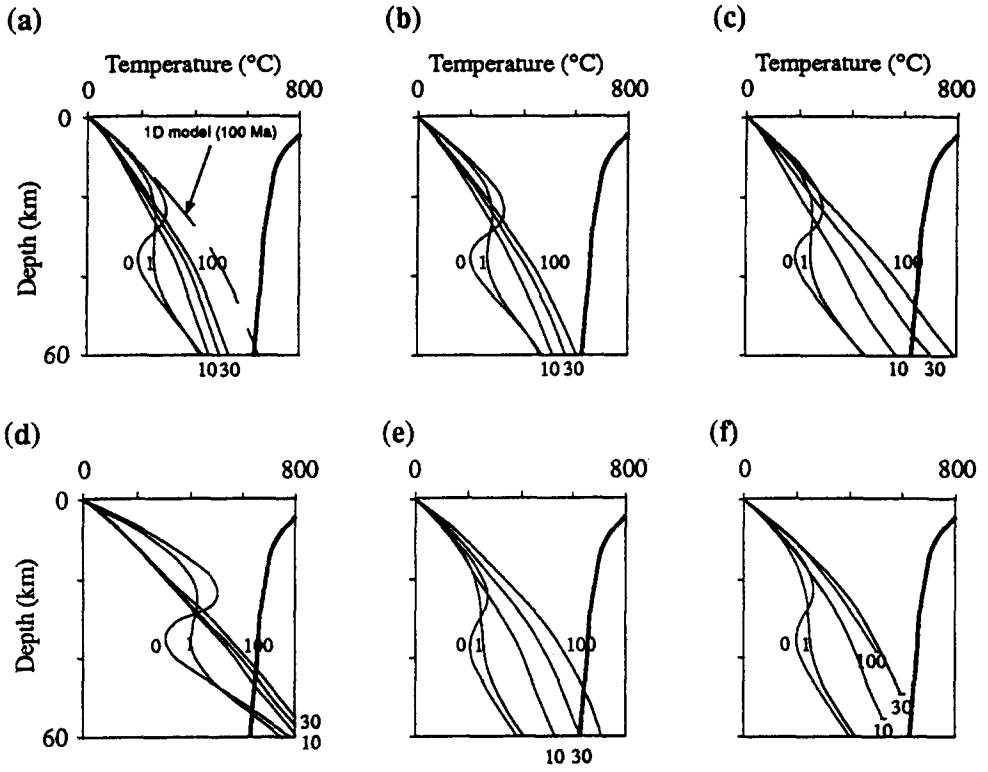

Fig. 8. Analysis of the model parameters. Temperature–depth profiles 0, 1, 10, 30 and 100 Ma after thrusting by which time the system has virtually attained its new equilibrium position. (a) Non-isostatic model depicted in Fig. 6b using average present-day thermal parameters with an exponential decrease in heat-producing elements. Initial parameters: $A_0 = 2.4\ \mu W\ m^{-3}$, $D = 10$ km, $Q_m = 29$ mW m^{-2}. (b) Same as (a) but with a uniform distribution of radiogenic material, resulting in the same surface heat flow ($Q_s = 52$ mW m^{-2}), and reduced heat flow (Q_m), as in (a). Initial parameters: $A = 0.77\ \mu W\ m^{-3}$ (uniform throughout the whole crust), $Q_m = 29$ mW m^{-2}. (c) Same as (a) but assuming that the reduced heat flow remains constant throughout the 100 Ma of thermal relaxation. Initial parameters: $A_0 = 2.4\ \mu W\ m^{-3}$, $D = 10$ km, $Q_m = 29$ mW m^{-2}. (d) Same as (a) but assuming a higher initial reduced surface heat flow, comparable to the Basin and Range in the United States. Initial parameters: $A_0 = 2.4\ \mu W\ m^{-3}$, $D = 10$ km, $Q_m = 60$ mW m^{-2}. (e) Isostatic model depicted in Fig. 6c using average present-day thermal parameters with an exponential decrease in heat-producing elements. Initial parameters: $A_0 = 2.4\ \mu W\ m^{-3}$, $D = 10$ km, $Q_m = 29$ mW m^{-2}. (f) Same as (e) but assuming that surface material is removed by erosion at a constant rate of 0.3 mm a^{-1}.

mantle constant throughout the 100 Ma time span of the model. Comparison with Fig. 8a shows that temperatures at depth are raised significantly and conditions for partial melting exist in the crust below 50 km after 100 Ma.

6.4. Reduced heat flow Q_m

One of the most sensitive constraints on the temperature distribution throughout the crust is the reduced heat flow Q_m. A comparison of Fig. 8d with Fig. 8a shows how doubling the initial value of this parameter alters the geotherms from the end of thrusting through to 100 Ma later. A higher value of Q_m increases the temperatures generated following crustal thickening, decreases the minimum depth of crustal melting and increases the quantity of melt. With a value of $Q_m = 60$ mW m^{-2} (a value corresponding to the Basin and Range, U.S.), crustal melting can occur at depths greater than 45 km after 100 Ma, with Moho temperature reaching 900°C.

6.5. Isostasy

Neglecting any isostatic effects creates a huge topographic relief of 30 km (unrealistic in geolog-

ical terms) created by the crustal-scale thrust slice shown in Fig. 6b. This generates significant horizontal temperature gradients which are ignored by 1D models. However, by including isostatic (Airy) equilibrium, this relief is reduced considerably, as shown in Fig. 6c. The major effect of isostasy on the thermal structure of the lithosphere is to reduce the horizontal temperature gradients significantly in the centre of the model and, as shown in Fig. 8e, a higher Moho temperature results than in the equivalent non-isostatic model, Fig. 8a. A comparison of these figures shows that Moho temperature after 100 Ma is increased from ~420°C to ~700°C, rather than from 420°C to 540°C, thus taking it to temperatures high enough to initiate crustal melting in the lowermost 5 km of the crust.

6.6. Erosion

So far in this analysis the effects of erosion have been neglected. However, the surface material in the hangingwall of the thrust will be uplifted, even in isostatic equilibrium, and removed by erosion. Erosion will have the effect of unloading the lithosphere and creating further isostatic uplift. Applying a constant erosion rate of 0.3 mm a^{-1} to the model of Fig. 6c removes 30 km of crustal material in 100 Ma, thinning the crust accordingly. Fig. 8f shows how the erosive removal of surface material decreases the maximum temperatures generated at the base of the crust, which in this case are insufficient to initiate partial melting.

7. Implications for large-scale anatexis

Using typical values for the heat flow at the Moho and a realistic radiogenic heat producing distribution throughout the crust, 2D thermo-mechanical modelling of the entire lithosphere under lateral compression has shown that Moho temperatures fall short of those required for extensive crustal melting if we include the effects of erosion. Our models have shown that for partial melting of the crust to occur, a 'hotter' initial geotherm is required. Assuming it to be an equilibrium geotherm, this can be achieved by: (1) increasing the reduced heat flow, Q_m; and/or (2) increasing the rate of radiogenic heating in the crust (i.e., increasing A_0). One mechanism by which the way reduced heat flow may be increased is if the continental collision followed shortly after a period of rifting which thinned the lithosphere, as is believed to have occurred in the southwestern United States during the Early Proterozoic (see Fig. 2). Another factor which must be taken into account here is that of radioactive decay. During the Early Proterozoic the value of radiogenic heating in the crust, A_0, was considerably higher than at present, simply because the Earth was that much younger and there had been less time for radioactive decay.

So far we have only considered elevated lower-crustal temperatures in the form of a 1D geotherm taken from the centre of the models in Fig. 6. Illustrated in Fig. 9 are three 2D temperature profiles across a region of thickened crust, neglecting the effects of erosion, 100 Ma after the end of thrusting. Fig. 9a represents a typical present-day geotherm using the average values in Table 2; Fig. 9b assumes a higher rate of radiogenic heating at the surface of the Earth than the present-day average; Fig. 9c was calculated using a higher initial reduced heat flow (representing a thinned lithosphere). These profiles illustrate not only the total volume of potential partial melt we would expect, but also its distribution across the orogenic belt. In regions of relatively thin lithosphere (Fig. 9c), elevated temperatures exist right across the region of thickened crust. In a region with a high rate of radiogenic heating, however (Fig. 9b), the elevated temperatures are more concentrated towards the centre of the belt. The models enable us to calculate a P–T–t path for any point within them. Fig. 10 illustrates three such paths of a point at the Moho in the centre of the model for the three different cases in Fig. 9 but including the assumption of a constant rate of erosion (0.3 mm a^{-1}). By 100 Ma the system has reached its new isostatic equilibrium position, with Moho at a depth of 38 km (for an initial lithospheric thickness of 110 km), providing that a mantle lithosphere root still exists, effectively acting as a heavy weight pulling down on the crust. In all cases the maximum temperatures are generated approximately 30 Ma after the end of thrusting, occurring at a depth of ~48 km. These anticlockwise paths show that we would only expect to see water-saturated crustal melting occurring if there is a higher rate of radiogenic heating in the crust than the present-day average, as is believed to

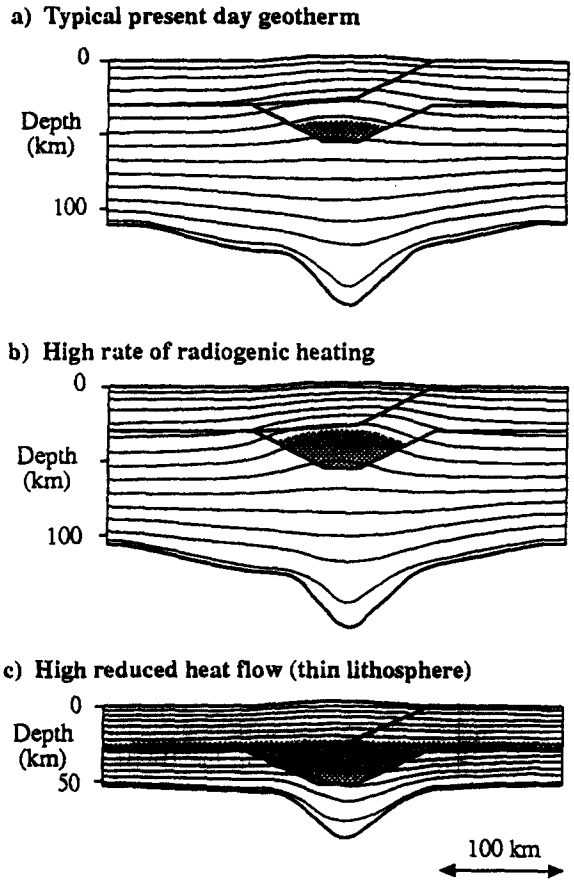

Fig. 9. Isostatic models illustrating temperature distribution, and the amount of potential crustal melt (indicated by the shaded regions), throughout the lithosphere 100 Ma after thrusting. (a) Average present-day thermal parameters. Initial conditions: $A_0 = 2.4\ \mu W\ m^{-3}$, $D = 10$ km, $Q_m = 29$ mW m^{-2}. (b) Increased rate of radiogenic heating within the crust. Initial conditions: $A_0 = 4\ \mu W\ m^{-3}$, $D = 10$ km, $Q_m = 29$ mW m^{-2}. (c) Increased value for the reduced heat flow, Q_m. Initial conditions: $A_0 = 2.4\ \mu W\ m^{-3}$, $D = 10$ km, $Q_m = 60$ mW m^{-2}.

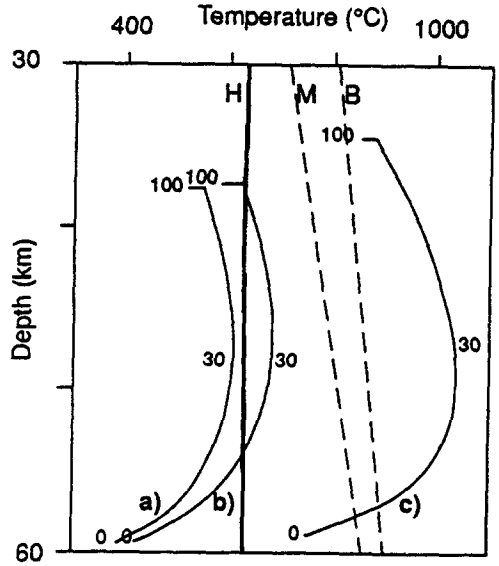

Fig. 10. Effects of erosion. *P–T–t* paths for the Moho in the centre of the thickened crust using the isostatic model, Fig. 6c, and assuming that surface material is removed at a constant rate of 0.3 mm a^{-1}. Numbers indicate time in Ma after thrusting has occurred. Curve *(a)*, average present-day parameters. Initial conditions: $A_0 = 2.4\ \mu W\ m^{-3}$, $D = 10$ km, $Q_m = 29$ mW m^{-2}. Curve *(b)*, high rate of radiogenic heating at the surface. Initial conditions: $A_0 = 4.0\ \mu W\ m^{-3}$, $D = 10$ km, $Q_m = 29$ mW m^{-2}. Curve *(c)*, thinned lithosphere. Initial conditions: $A_0 = 2.4\ \mu W\ m^{-3}$, $D = 10$ km, $Q_m = 60$ mW m^{-2}.

have existed in Precambrian times. For fluid-absent melting to occur, however, higher temperatures still are required, such as those generated by a higher reduced heat flow of 60 mW m^{-2} (curve 10c) in order to intersect the temperature–depth curves representing the breakdown of muscovite (M) and biotite (B) in metapelite.

Evidence from deep seismic and gravity data, however, suggests that the erosive effect may not be as significant as we have predicted here. For example, beneath the Himalayas there exists a thickened crust in excess of 60 km some 45 Ma after the initial collision. Hence, when investigating orogenic belts which have been shortening for large periods of time, the models presented in Fig. 9 may be more applicable than those in Fig. 10 which include erosion — in this case we would then expect to see a small amount of crustal melting using average present-day thermal parameters (Fig. 9a), and this may have been the mechanism responsible for the formation of some of the Himalayan leucogranites.

8. Conclusions

By including a realistic variation of radioactive heat production with depth and, above all, including the thickening of the upper mantle part of the lithosphere as well as the crust, in a 2D model of an orogenic belt, it is clear that previously published models substantially overestimated the rise in temperatures that would be created in a region of

thickened crust. 1D models which take no account of lateral temperature gradients may generate quite different temperatures at the base of the crust than the 2D equivalent — the lower temperatures on the periphery of the orogenic belt in the latter case reducing the effects of increased radiogenic heating. A decrease in the radioactive heating production rate throughout the crust also reduces predicted temperatures in the lower crust — an effect which is accentuated further with the erosive removal of the higher-radioactive materials at the Earth's surface. Another significant effect comes from thickening of the mantle portion of the lithosphere.

In typical continental areas with lithospheric thicknesses in excess of 140 km, crustal thickening is unlikely to generate a significant amount of crustal melt granites just as a result of increased radiogenic heating produced by thrusting. In modern orogenic belts resulting from collision of continental lithosphere of normal thickness, the heat to initiate melting must come from elsewhere. One possibility, which has been suggested by numerous authors (e.g., Nelson, 1992), is from delamination of the mantle lithosphere. It has been proposed that, following lithospheric thickening, the relatively dense upper mantle lithospheric root becomes detached from the crust and sinks into the underlying asthenosphere. This would allow high-temperature asthenosphere to reach the base of the crust and thus rapidly increase Q_m, the reduced heat flow. The effect of this would then be similar to that depicted in Fig. 9c in which elevated temperatures arise.

The models presented in this analysis have assumed that crustal shortening has been accommodated by a single thrust sheet. Deep seismic profiles (e.g., Fig. 3) indicate a suite of imbricated thrust sheets. However, it seems unlikely that the crust could be thickened by more than a factor of two (also supported by seismic evidence, see Fig. 1) used in our models. If a suite of thrusts were to form, the mantle lithosphere would also deform across the lateral width of the suite, which would have the effect of lowering the reduced heat flow Q_m even more than in our analysis, so our results represent the maximum temperatures to be expected. In our models, the mantle lithosphere is deformed by a pure shear mechanism symmetrically beneath the crustal thrust. Evidence from seismic and gravity data suggests that upper mantle lithosphere may be subducted asymmetrically (e.g., Fig. 1c) and is offset laterally from the overlying mountain belt and thickened crust, but this still leads to the formation of a lithospheric root beneath the thickened crust. Only if the lateral offset is very great will the temperature distribution in the crust be significantly perturbed.

Our models predict that heating of the crust as a consequence of shortening and thickening of continental lithosphere can only initiate extensive partial melting at the present time in exceptional circumstances, such as in regions of relatively thin lithosphere or where there is an unusually large rate of radiogenic heating within the crust. Otherwise, delamination of mantle lithosphere is needed. The models also show the likeliest locations within the crust and the time scales over which melting could occur, and allow calculation of P–T–t pathways for any point within them.

Acknowledgements

The authors are grateful to the European Commission and BIRPS for support in the BABEL project. BIRPS deep seismic reflection profiles are provided under the authority of the NERC to whom grateful acknowledgement is made. JPM is grateful to Chris Willacy (RHUL) for assistance with the development of the initial thermal models and to the NERC for the provision of a scholarship.

References

Andersson, U.B., 1991. Granitoid episodes and mafic–felsic magma interaction in the Svecofennian of the Fennoscandian shield, with main emphasis on the ~1.8 Ga plutonics. Precambrian Res., 51: 127–149.

Ansorge, J., Blundell, D. and Mueller, St., 1992. Europe's lithosphere — seismic properties. In: D. Blundell, R. Freeman and St. Mueller (Editors), A Continent Revealed: the European Geotraverse. Cambridge University Press, Cambridge, pp. 33–65.

BABEL Working Group, 1993. Deep seismic reflection/refraction interpretation of crustal structure along BABEL profiles A and B in the southern Baltic Sea. Geophys. J. Int., 112: 325–343.

Bayer, R., Cazes, M., Dal Piaz, G.V., Damotte, B., Elter, G., Gosso, G., Hirn, A., Lanza, R., Lombardo, B., Mugnier, J.-L., Nicolas, A., Nicolich, R., Polino, R., Roure, F., Sacchi, R., Scarascia, S., Tabacco, I., Tapponnier, P., Tardy, M., Taylor, M., Thouvenot, F., Torreilles, G. and Villien, A., 1987.

Premiers résultats de la traversé des Alpes occidentales par seismique reflexion verticale (Programme ECORS-CROP). C. R. Acad. Sci., Paris, 305: 1461–1470.

BIRPS and ECORS, 1988. Deep seismic profiling between England, France and Ireland. J. Geol. Soc. London, 143: 45–52.

Butler, R.W.H. and Coward, M.P., 1989. Crustal scale thrusting and continental subduction during Himalayan collision tectonics of the NW Indian Plate. In: A.M.C. Sengor (Editor), Tectonic Evolution of the Tethyan Region. NATO ASI Ser., C, 259: 387–413.

Carslaw, H.S. and Jaeger, J.C., 1959. Conduction of Heat in Solids, 2nd Ed. Oxford University Press, New York.

Condie, K.C., 1982. Plate-tectonics model for Proterozoic continental accretion in the southwestern United States. Geology, 10: 37–42.

Cook, F.A., Varsek, J.J., Clowes, R.M., Kanasewich, E.R., Spencer, C.S., Parrish, R.R., Brown, R.K., Carr, S.D., Johnson, B.J. and Price, R.A., 1992. Lithoprobe crustal reflection cross section of the southern Canadian Cordillera, 1. Foreland thrust and fold belt to Fraser River Fault. Tectonics, 11: 12–35.

Coward, M.P. and Butler, R.W.H., 1985. Thrust tectonics and the deep structure of the Pakistan Himalaya. Geology, 13: 417–420.

Dewey, J.F., Shackleton, R.M., Chang Chengfa and Sun Yujin, 1988. The tectonic evolution of the Tibetan Plateau. Philos. Trans. R. Soc. London, Ser., A, 327: 379–413.

Dewey, J.F., Cande, S. and Pitman, W.C., 1989. Tectonic evolution of the India/Eurasia collision zone. Eclog. Geol. Helv., 82: 717–734.

England, P.C. and Molnar, P., 1990. Right lateral shear and rotation as the explanation for strike slip faulting in eastern Tibet. Nature, 344: 140–142.

England, P.C. and Thompson, A., 1986. Some thermal and tectonic models for crustal melting in continental collision zones. In: M.P. Coward and A.C. Ries (Editors), Collision Tectonics. Geol. Soc. London, Spec. Publ., 19: 83–94.

Graham, C.M. and England, P.C., 1976. Thermal regimes and regional metamorphism in the vicinity of overthrust faults: an example of shear heating and inverted metamorphic zonation from southern California. Earth Planet. Sci. Lett., 31: 142–152.

Green, A.G., Milkereit, B., Davidson, A., Spencer, C., Hutchinson, D.R., Cannon, W.R., Lee, M.W., Agena, W.F., Behrendt, J.C. and Hinze, W.J., 1989. Crustal structure of the Grenville Front and adjacent terranes. Geology, 16: 788–792.

Huang, W.L. and Wyllie, P.J., 1981. Phase relationship of S-type granite with H_2O to 35 kbar: Muscovite granite from Harney Peak, South Dakota. J. Geophys. Res., 86: 1015–1029.

Johnston, D.C. and White, S.H., 1983. Shear heating associated with movement along the Alpine Fault, New Zealand. Tectonophysics, 92: 241–252.

Laubscher, H.P., 1983. Detachment, shear and compression in the Central Alps. Geol. Soc. Am. Mem., 158: 191–211.

Laubscher, H., 1992. The Alps — a transpressive pile of peels. In: K.R. McClay (Editor), Thrust Tectonics. Chapman and Hall, London, pp. 277–285.

Le Breton, N. and Thompson, A.B., 1988. Fluid-absent (dehydration) melting of biotite in metapelites in the early stage of crustal anatexis. Contrib. Mineral. Petrol., 99: 226–237.

Mattauer, M., 1986. Intracontinental subduction, crust–mantle decollements and crustal-stacking wedge in the Himalayas and other collision belts. In: M.P. Coward and A.C. Ries (Editors), Collision Tectonics. Geol. Soc. London, Spec. Publ., 19: 37–50.

Muñoz, J.A., 1992. Evolution of a continental collision belt: ECORS-Pyrenees crustal balanced cross-section. In: K.R. McClay (Editor), Thrust Tectonics. Chapman and Hall, London, pp. 235–246.

Nelson, K.D., 1992. Are crustal thickness variations in old mountain belts like the Appalachians a consequence of lithospheric delamination? Geology, 20: 498–501.

Ruppel, C. and Hodges, K.V., 1994. Role of horizontal thermal conduction and finite time thrust emplacement in simulation of pressure–temperature–time paths. Earth Planet. Sci. Lett., 123: 49–60.

Sclater, J.G., Jaupart, C. and Galson, D., 1981. The heat flow through oceanic and continental crust and the heat loss of the earth. Rev. Geophys. Space Phys., 18: 269–311.

Shi, Y. and Wang, C., 1987. Two-dimensional modeling of the *P–T–t* paths of regional metamorphism in simple overthrust terrains. Geology, 15: 1048–1051.

Treloar, P.J., Coward, M.P., Chambers, A.F., Izatt, C.N. and Jackson, K.C., 1992. Thrust geometries, interferences and rotations in the Northwest Himalaya. In: K.R. McClay (Editor), Thrust Tectonics. Chapman and Hall, London, pp. 325–342.

Waltham, D. and Hardy, S., 1995. The velocity description of deformation. Paper 1: Theory. Mar. Pet. Geol., 12: 153–163.

Windley, B., 1992. Tectonic evolution of Europe. In: D. Blundell, R. Freeman and St. Mueller (Editors), A Continent Revealed: the European Geotraverse. Cambridge University Press, Cambridge, pp. 139–214.

Wyllie, P.J., 1992. Experimental petrology: Earth materials science. In: G.C. Brown, C.J. Hawkesworth and R.C.L. Wilson (Editors), Understanding the Earth, a New Synthesis. Cambridge University Press, Cambridge, pp. 67–87.

Zuber, J.A. and Öhlander, B., 1990. Geophysical and geochemical evidence of Proterozoic collision in the western marginal zone of the Baltic Shield. Geol. Rundsch., 79: 1–11.